Quantum Optimization for Closed-Loop Scheduling of Earth Observation Satellite Formation

SN Computer Science (2025) 6:739
https://doi.org/10.1007/s42979-025-04252-2

ORIGINAL RESEARCH

Quantum Optimization for Closed-Loop Scheduling of Earth Observation Satellite Formation

Vinicius Marchioli[1] · Mattia Boggio[1] · Deborah Volpe[1] · Luca Massotti[2] · Carlo Novara[1]

Received: 16 December 2024 / Accepted: 21 July 2025

Abstract

The scheduling complexity of Agile Earth Observation Satellites (AEOSs) increases significantly as Earth Observation missions progress. This makes traditional optimization techniques less effective, restricting their application to small-scale and open-loop scheduling problems. In this paper, we investigate the potential of quantum solvers to address the closed-loop scheduling problem for a formation of AEOSs, overcoming the limitations of classical optimization techniques. To this end, we formulate the scheduling problem as a novel Quadratic Unconstrained Binary Optimization (QUBO) problem, i.e., a formulation specifically designed for quantum solvers. Moreover, penalty functions are introduced to minimize mission energy consumption and reduce deviations between the original and rescheduled solutions. The formulated QUBO problem is implemented on a D-Wave quantum annealer for a daily and large-scale scheduling scenario. The obtained results demonstrate significant improvements in computational efficiency and solution quality compared to traditional methods like Simulated Annealing and Tabu Search, highlighting the potential of quantum solvers in optimizing complex scheduling tasks for AEOS formations.

Keywords Quantum optimization · QUBO · Earth observation mission · Closed-loop satellite formation scheduling

Introduction

With the increasing accessibility of space exploration, Earth Observation (EO) missions have become a critical area for scientific research and strategic applications [1, 2], including studying natural phenomena [3–5] and climate change [1, 6], as well as improving national security through border and resource monitoring [7]. In this context, Agile Earth Observation Satellites (AEOSs) represent a significant advancement in EO missions by offering enhanced flexibility and precision [8, 9]. Operating in Low Earth Orbit (LEO), often as part of constellations, these satellites feature an additional degree of freedom around the pitch axis, enabling fast and accurate orientation changes in nadir (see Fig. 1a). Unlike traditional Earth Observation Satellites (EOS), where the Observation Time Window (OTW) is inherently limited to coincide with the Visible Time Window (VTW), AEOSs can identify multiple OTWs within a single VTW (see Fig. ,1b). This capability expands their operational range and improves their efficiency in observing high-priority targets.

However, the increased agility of AEOSs introduces significant challenges in the scheduling problem for EO missions. This problem consists of selecting and scheduling satellite observation tasks to maximize the entire observation profit while satisfying all the operational constraints. In conventional EOS systems, scheduling is relatively straightforward since the OTW and VTW coincide. By contrast, the flexibility of AEOSs to select from multiple OTWs within a single VTW exponentially increases the search space for scheduling solutions. This complexity makes the scheduling problem NP-hard [10], posing a significant challenge

✉ Mattia Boggio
mattia.boggio@polito.it

Vinicius Marchioli
vinicius.marchioli@studenti.polito.it

Deborah Volpe
deborah.volpe@polito.it

Luca Massotti
luca.massotti@esa.int

Carlo Novara
carlo.novara@polito.it

[1] Politecnico di Torino, Corso Duca degli Abruzzi 24, 10124 Turin, Italy

[2] European Space Agency, Keplerlaan 1, 2201 AG Noordwijk, The Netherlands

Published online: 12 August 2025

Fig. 1 Agile Earth Observation Satellites (AEOSs)

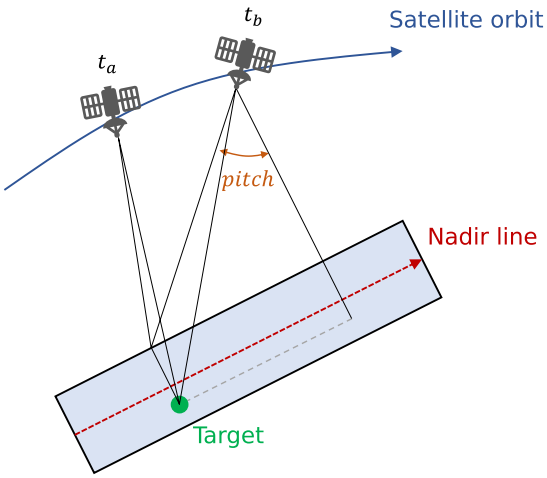

(a) AEOS's enhanced manoeuvrability around the pitch axis.

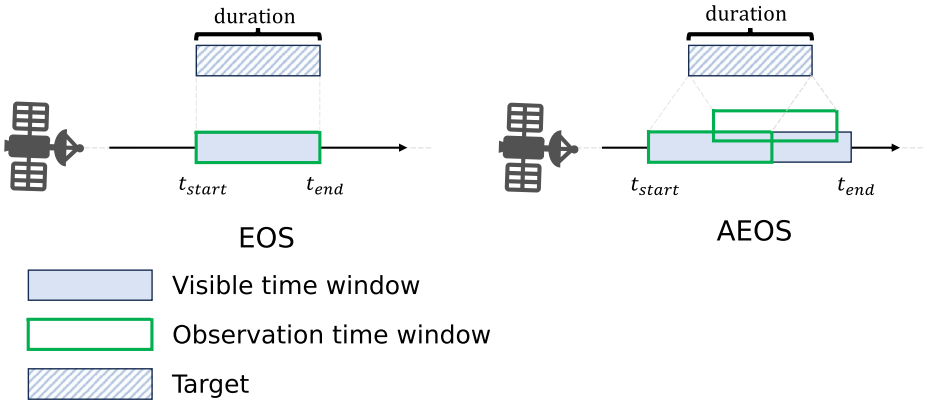

(b) Comparison of the observation capability of EOS and AEOS.

for conventional optimization techniques. Indeed, traditional methods may struggle to identify globally optimal solutions or may require prohibitive computational times, especially in the case of satellite constellations or as the number of potential observations increases.

Consequently, traditional methods are often restricted to open-loop scheduling, where complete information about the problem and a static environment are assumed (see, e.g., [11–13]). However, real-world satellites operate in complex environments with various uncertainties like satellite defects or malfunctions, new tasks, or unexpected cloud cover. As a result, precomputed schedules are rarely executed as planned, requiring closed-loop scheduling for AEOS [14–16]. This type of scheduling allows real-time responses to potential changes in the mission scenario, such as those arising from emergency conditions, including natural disaster monitoring, industrial accidents, or public health crises.

This paper addresses the problem of closed-loop scheduling for a formation[1] of satellites considering a large number of targets. Given the limitations of traditional approaches, we adopt an innovative computational paradigm, i.e., the quantum computing. In recent years, quantum computing has gained significant attention and popularity due to its potential to significantly improve the efficiency and quality of solutions to complex optimization problems [17, 18].

The nowadays literature has provided substantial demonstrations of the use of quantum annealers to address real-world optimization challenges [19–26]. In the realm of aerospace applications, the optimization of scheduling problems for EO missions has emerged as an area of growing research interest for quantum computing. Pioneering work on this topic can be found in [27, 28]. In particular, [28] proposes the use of a quantum annealer, specifically

[1] The term constellation is referred to a general scenario, while formation is specific to the closed-loop case.

employing a Hybrid Quantum Annealing (HQA) algorithm [29], for scheduling problem of AEOS constellations. The study formulates this problem as a Quadratic Unconstrained Binary Optimization (QUBO) problem, providing a comprehensive formulation for a constellation of multiple satellites. To reduce propellant consumption and extend mission lifetime, penalty functions are integrated into the optimization process. The QUBO problem is implemented and solved on a real quantum annealer, conducting extensive simulations. The results are compared with state-of-the-art QUBO solvers running on classical computers, such as Simulated Annealing (SA) [30] and Tabu Search (TS) [31], showing the potential of hybrid quantum-classical algorithms to solve complex scheduling problems more efficiently than traditional methods.

The research gaps addressed by this article are the following:

1. Formulation of the closed-loop scheduling problem of AEO satellite formations and translation into a QUBO problem: in this case, we include the capability to dynamically reschedule operations in response to unexpected events, such as satellite malfunctions;
2. Integration of penalty functions in the optimization problem for minimizing the deviations between the original schedule and the rescheduled solution: in the event of satellite defects, it is important to handle dynamic rescheduled operations with minimal changes with respect to the initial scheduling;
3. Use of an extensive dataset comprising a large number of observation targets: this enables the simulation of a realistic daily scheduling scenario for EO mission, taking into account multiple orbital revolutions;
4. Implementation and solution of the obtained QUBO problem on a real quantum annealer, showing significant advantages in terms of both computational efficiency and solution quality compared to classical approaches such as SA and TS.

To the best of our knowledge, this is the first study to address such a realistic and comprehensive EO closed-loop scheduling problem through the use of quantum paradigms. A graphical representation of the developed approach is presented in Fig. 2.

This article is organized as follows. "Formation Closed-Loop Scheduling Problem" introduces the mathematical formulation of the closed-loop formation scheduling problem. "QUBO Formulation" details the translation of this formulation into a QUBO problem. In "Solvers", the classical and quantum solvers, used for the resolution of the scheduling problem, are presented. The mission scenario for the EO scheduling problem is described in "Mission Scenario Description". "Simulation Results" presents a comparative analysis of the results obtained using the quantum annealer and classical solvers. Finally, the conclusions are drawn in "Conclusions".

Formation Closed-Loop Scheduling Problem

Consider a formation of N_S satellites traveling on different orbits. The three-satellite formation, considered in this study and characterized by heliosynchronous, highly polar, circular orbits, is depicted in Fig. 3a and b. In particular, Fig. 3a depicts a single revolution over the globe, while Fig. 3b shows the complete orbits over 24 h. It should be noted that the QUBO formulation developed in this paper is general and does not depend on the specific characteristics of the formation considered. For demonstration purposes, the SuperView-1 formation [32], which consists of Chinese commercial and remote sensing satellites, is used as a case study. Although Satellites 2 and 3 share similar orbits, they can be used to observe different targets, thereby reducing fuel consumption. For more details, please refer to "Mission Scenario Description" and "Simulation Results".

The orbits are designed in such a way that an arc of each orbit lies above a given region of the Earth containing N_T targets. When a satellite is traveling in its orbit, it spends a

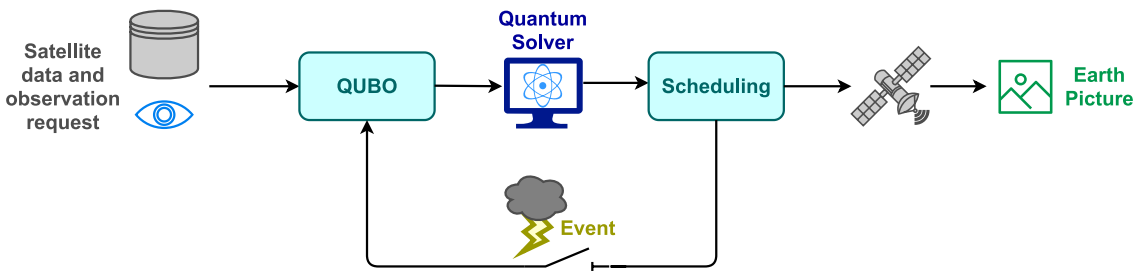

Fig. 2 Block diagram representing the closed-loop scheduling mechanism for Agile Earth Observation Satellites (AEOS). The workflow includes QUBO problem formulation, quantum or classical solver, and the rescheduling mechanism to adapt to real-time changes, such as climate or updated priorities

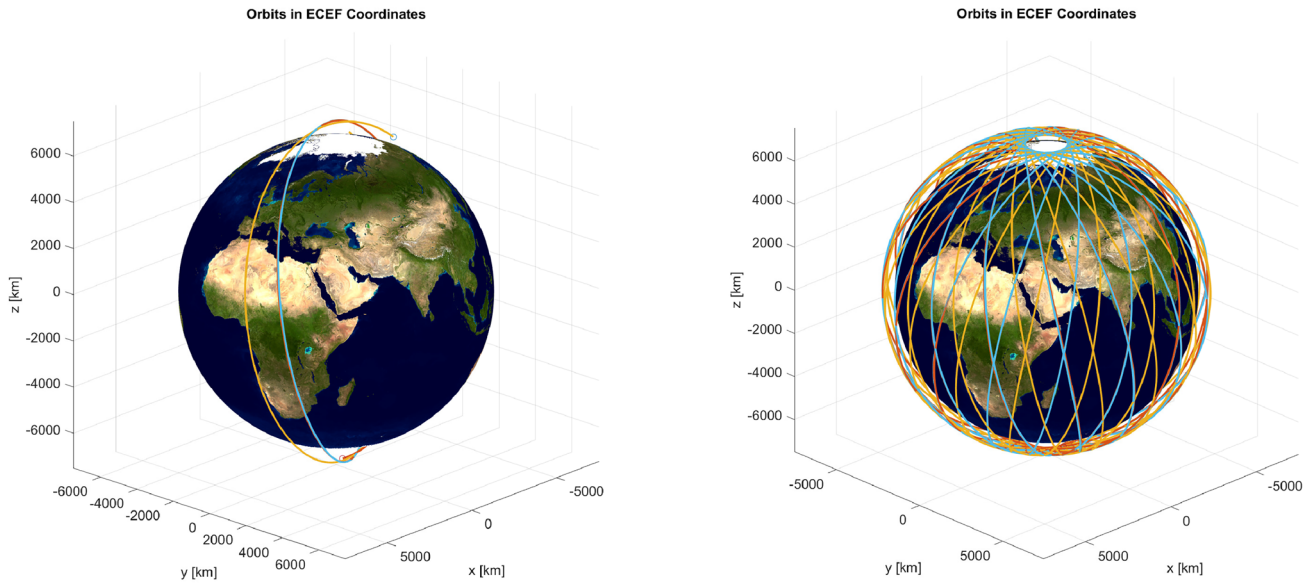

(a) Single orbital revolution. (b) Daily orbital revolutions.

Fig. 3 Example of a three-satellite formation, characterized by heliosynchronous, highly polar, circular orbits

fraction of the orbit period on the arc above the region and, in this time interval, it can acquire observations/images of the targets. The fraction of the orbit period spent on the arc is called Visible Time Window (VTW). The orbit arc is divided into smaller segments, corresponding to sub-intervals of duration ΔT of the VTW. While flying on a segment, a satellite can acquire observations of a subset of targets. Over 24 h, 15 orbital revolutions are considered, so a target may be visible many times by a satellite. The goal is to find an optimal observation scheduling for the satellites of the formation. To formalize the optimization problem, the following quantities are defined:

- $S \doteq \{1, \dots, N_S\}$: Satellite index set. An index $j \in S$ indicates the jth satellite of the formation.
- $T \doteq \{1, \dots, N_T\}$: Target index set. An index $i \in T$ indicates the ith target.
- $VTW_{ji}, i \in T, j \in S$: Orbit segment index set. VTW_{ji} contains the indices associated to the orbit segments from which the jth satellite can acquire an image of the ith target. The indices in VTW_{ji} are ordered by increasing traveling time.
- $w_{jik} \in \mathbb{R}_{\geq 0}$, $j \in S$, $i \in T$, $k \in VTW_{ji}$: Profit associated to a target. w_{jik} is related to the priority of acquiring an image of the ith target. The priority may depend on the satellite and the orbit segment.
- $\xi_{jik} \in \{0, 1\}$, $j \in S$, $i \in T$, $k \in VTW_{ji}$: Decision variable. ξ_{jik} indicates if the jth satellite has acquired an image of the ith target while flying in the orbit segment with index $k \in VTW_{ji}$. $\xi_{jik} = 1$ if the acquisition has been accomplished, $\xi_{jik} = 0$ otherwise.
- $n = \sum_{j=1}^{N_S} \sum_{i=1}^{N_T} \text{card}(VTW_{ji})$: Number of decision variables $\xi_{jik} \in \{0, 1\}$. Note that, in general, $n \leq N_S N_T$.
- $\zeta \doteq (\xi_{j_1 i_1 k_1}, \dots, \xi_{j_n i_n k_n}) \in \{0, 1\}^n \subset \mathbb{N}^{n \times 1}$, $j_1, \dots, j_n, \in S$, $i_1, \dots, i_n \in T$, $k_1 \in VTW_{j_1 i_1}, \dots$ $k_n \in VTW_{j_n i_n}$: Vector containing all the decision variables. The order in which the ξ_{jik}'s appear in ζ is arbitrary. The one adopted in this paper is as follows: $ijk \in \{111, 112, \dots, 121, 122, \dots, 211, 212, \dots, 221, 222, \dots\}$. The symbol $\mathbb{N}$ denotes the set of natural numbers including 0.

Based on these definitions, the ideal profit of the whole mission is

$$J_P \doteq \sum_{i \in T} \sum_{j \in S} \sum_{k \in VTW_{ji}} w_{jik} \xi_{jik}.$$

In this work, we have chosen to make a single acquisition for each target in order to avoid excessive fuel consumption. This can be imposed by the following constraints:

$$\sum_{j \in S} \sum_{k \in VTW_{ji}} \xi_{jik} \leq 1, \quad \forall i \in T. \tag{1}$$

It must also be taken into account that the observation of two consecutive targets may not be feasible, since there may not be enough time for a satellite to maneuver from one

acquisition to the subsequent one. To prevent the scheduling of consecutive observations that cannot be completed, the following constraints are introduced:

$$\begin{aligned} &\xi_{ji_1k_1} + \xi_{ji_2k_2} \leq 1, \quad \forall j \in S, \\ &\forall i_1, i_2 \in T, i_1 \neq i_2, \forall (k_1, k_2) \in F_{ji_1i_2}, \end{aligned} \tag{2}$$

where $F_{ji_1i_2}$ denotes the *unfeasible maneuver region*, defined as the set of segment indices (k_1, k_2) where the interval between the end of the first acquisition and the start of the second one is insufficient for the required maneuver. Formally, this set is expressed as:

$$\begin{aligned} F_{ji_1i_2} \doteq \{&(k_1, k_2) \in VTW_{ji_1} \times VTW_{ji_2} \ : \\ &\tau_{ji_2k_2} < \tau_{ji_1k_1} + T_F\}, \end{aligned}$$

where τ_{jik} is the start time of the ith target acquisition, accomplished by the jth satellite from the kth orbit segment, and T_F is the sum of the duration of an acquisition and the duration of the maneuver.

In order to penalize acquisitions which require a high attitude adjustment and thus a high fuel consumption, the following term is introduced:

$$J_C \doteq \sum_{i \in T} \sum_{j \in S} \sum_{k \in VTW_{ji}} \lambda_{jik} \xi_{jik}.$$

One of the main contributions of this paper is the ability to execute closed-loop scheduling when a reprogramming operation is required due to the presence of unexpected events, as shown in Fig. 2. For energy saving reasons, to ensure that the new schedule does not have too large variations with respect to the previous one, the old solution ξ_{ijk}^{old} is used to penalize significantly different outcomes:

$$J_R \doteq \sum_{i \in T} \sum_{j \in S} \sum_{k \in VTW_{ji}} \lambda_{jik} \left| \xi_{jik} - \xi_{jik}^{\text{old}} \right|,$$

which can be more adequately rewritten in binary form as:

$$J_R \doteq \sum_{i \in T} \sum_{j \in S} \sum_{k \in VTW_{ji}} \lambda_{jik} \left(\xi_{jik}(1 - 2\xi_{jik}^{\text{old}}) + \xi_{jik}^{\text{old}} \right).$$

This term makes the algorithm a closed-loop one, where the old variables ξ_{ijk}^{old} are used in a feedback manner to compute the new variables ξ_{ijk}.

Finally, the objective function is defined as:

$$J(\zeta) \doteq -J_P + J_C + J_R, \tag{3}$$

where $\zeta \doteq (\xi_{111}, \xi_{112}, \ldots, \xi_{121}, \ldots, \xi_{211}, \ldots, \xi_{N_s11}, \ldots)$. An optimal observation scheduling for the satellites of the formation can be found by solving the following optimization problem:

$$\begin{aligned} &\zeta^* = \arg \min_{\zeta \in \{0,1\}^n} J(\zeta) \\ &\text{subject to:} \\ &\text{(i)} \sum_{j \in S} \sum_{k \in VTW_{ji}} \xi_{jik} \leq 1, \quad \forall i \in T \\ &\text{(ii)} \ \xi_{ji_1k_1} + \xi_{ji_2k_2} \leq 1, \quad \forall j \in S, \\ &\quad \forall i_1, i_2 \in T, i_1 \neq i_2, \forall (k_1, k_2) \in F_{ji_1i_2}. \end{aligned} \tag{4}$$

In general, (4) is an Integer Linear Programming (ILP). Due to the discrete nature of the decision variables, this kind of problem is NP-hard for a classical computer. Quantum computers and, in particular, quantum annealers have the potential to significantly reduce the computational complexity of these classes of problems, finding better solutions with a polynomial speedup compared to classical computers [33]. A formulation of the optimization problem (4) that is compliant with quantum annealers is called QUBO (Quadratic Unconstrained Binary Optimization) and is developed in the next section.

QUBO Formulation

This section introduces our QUBO (Quadratic Unconstrained Binary Optimization) formulation for the closed-loop scheduling problem of the EO satellite formation described in Eq. (4). The QUBO model requires the objective function to be expressed in the following form:

$$H = \zeta^\top \mathbf{Q} \, \zeta, \tag{5}$$

where $\mathbf{Q} \in \mathbb{R}^{n \times n}$ is a matrix of real numbers and $\zeta \in \{0,1\}^n \subset \mathbb{N}^{n \times 1}$ is a vector of binary variables. This optimization model handles constraints only using an aggregation method, which incorporates quadratic penalty functions into the objective function. These functions assume a value of zero when the constraints are satisfied and take on positive values otherwise.

The operations needed to obtain the QUBO formulation (5) of the optimization problem (4) are now described in detail.

The function $J(\zeta)$ of Eq. (3) can be written as:

$$\begin{aligned} J &\doteq -J_P + J_C + J_R \\ &= \sum_{i \in T} \sum_{j \in S} \sum_{k \in VTW_{ji}} (2\lambda_{jik}(1 - \xi_{ijk}^{\text{old}}) - w_{jik})\xi_{jik} + \lambda_{ijk}\xi_{ijk}^{\text{old}} \\ &= \sum_{i \in T} \sum_{j \in S} \sum_{k \in VTW_{ji}} (2\lambda_{jik}(1 - \xi_{ijk}^{\text{old}}) - w_{jik})\xi_{jik}^2, \end{aligned}$$

where the constant term is neglected since it does not influence the minimum of the function and $\xi_{jik} = \xi_{jik}^2$, $\forall j, i, k$ is considered, knowing that ξ_{jik} is binary.

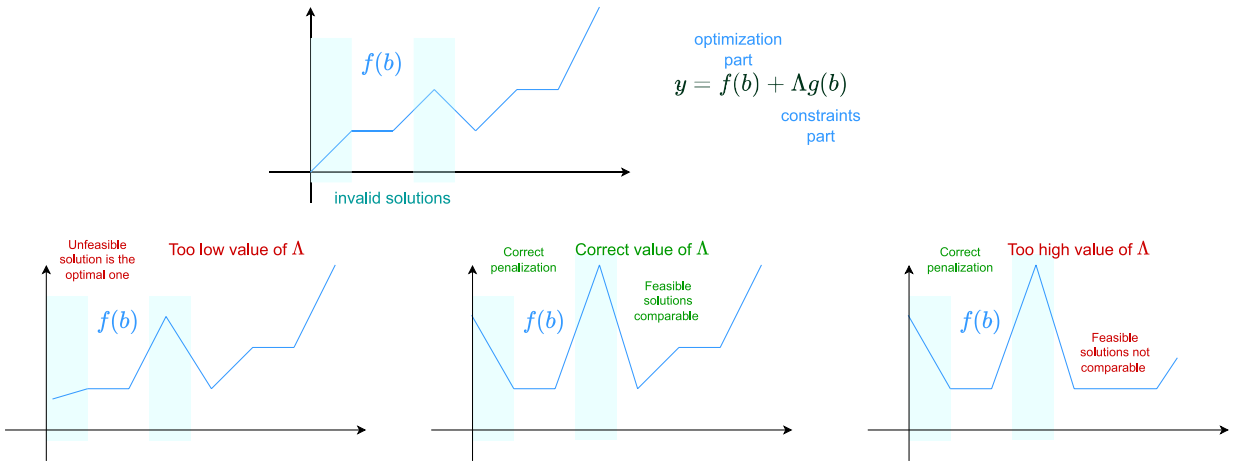

Fig. 4 Influence of Λ value on the solution quality. A too-low value (on the left) could give unreliable solutions because ones which do not satisfy the constraint are not correctly penalized with respect to the other. While a too-high value makes all solutions that satisfy the constraints equal from an energy point of view, thus implying that it is impossible to distinguish the optimal one for the $f(x)$ function

The constraints in Eq. (1) can be written through the following penalty functions:

$$\rho_i \doteq \frac{1}{2} \sum_{j_1,k_1 j_2,k_2} \xi_{j_1 i k_1} \xi_{j_2 i k_2}, \quad \forall i \in T,$$

for all $j_1, j_2 \in S, k_1 \in VTW_{j_1 i}, k_2 \in VTW_{j_2 i}, (j_2, k_2) \neq (j_1, k_1)$. It is possible to verified that $\rho_i = 0$ if and only if the constraint $\sum_{j \in S} \sum_{k \in VTW_{ji}} \xi_{jik} \leq 1$ is satisfied. Similarly, the constraints in Eq. (2) are represented by the following penalty terms:

$$\eta_l \doteq \xi_{ji_1k_1} \xi_{ji_2k_2}, \ \forall j \in S,$$
$$\forall i_1, i_2 \in T, i_1 \neq i_2, \forall (k_1, k_2) \in F_{ji_1i_2},$$

where $l = 1, \ldots, N_U$ and N_U is the number of unfeasible maneuvers. The penalties η_l are formulated in a QUBO-compliant format, specifically as quadratic functions. Their contributions define the off-diagonal elements of the $\mathbf{Q}$ matrix.

Including the penalties, the following objective function is obtained:

$$H \doteq -J_P + J_C + J_R + \Lambda \left(\sum_{i=1}^{N_T} \rho_i + \sum_{l=1}^{N_U} \eta_l \right), \tag{6}$$

where Λ is a positive real number. When appropriately chosen, Λ ensures that the minima of H correspond to the solutions of the optimization problem in Eq. (4). However, determining an appropriate value for Λ is non-trivial, as it must be large enough to penalize invalid solutions while avoiding excessive flattening of the problem function, which could hinder effective exploration of the solution space, as shown in Fig. 4. Tutorials [34] suggest taking Λ as a certain percentage of the original objective function (usually in the range **75–150%**). Unfortunately, estimating the function range is too complex, therefore, an effective value for Λ was found empirically.

While J_P represents the mission ideal profit, $-H$ accounts for the profit adjusted by penalties. Therefore, $-H$ is indicated as the Practical Profit.

From the quadratic function H of $\zeta = (\zeta_1, \ldots, \zeta_n) \doteq (\xi_{j_1 i_1 k_1}, \ldots, \xi_{j_n i_n k_n})$, the $\mathbf{Q}$ can be straightforwardly written. In practice, the coefficients $2\lambda_{jik}(1 - \xi_{ijk}^{\text{old}}) - w_{jik}$ of $J = -J_P + J_C + J_R$ are on the main diagonal of $\mathbf{Q}$, whereas the penalty terms ρ_i and η_l give off-diagonal entries equal to Λ. To be precise, let $q_{\alpha\beta}, \alpha, \beta = 1, \ldots, n$ be the entries of $\mathbf{Q}$. Then, $\mathbf{Q}$ is constructed as follows:

- $\text{diag}(\mathbf{Q}) = (p_{j_1 i_1 k_1}, \ldots, p_{j_n i_n k_n}), p_{jik} \doteq 2\lambda_{jik}(1 - \xi_{ijk}^{\text{old}}) - w_{jik}$.
- $q_{\alpha\beta} = \Lambda$ if, for some i, the term $\zeta_\alpha \zeta_\beta$ is contained in ρ_i, or, for some l, it is contained in η_l.
- $q_{\alpha\beta} = 0$ otherwise.

Afterwards, $\mathbf{Q}$ can be made symmetrical, if the solver requires this, by posing $\mathbf{Q} = (\mathbf{Q} + \mathbf{Q}^T)/2$.

Therefore, the resulting optimization problem is written in the QUBO form as follows:

$$\zeta^* = \arg \min_{\zeta \in \{0,1\}^n} \zeta^\top \mathbf{Q}\, \zeta. \tag{7}$$

For proper values of Λ, the solutions of (7) are also solutions of the optimization problem (4). The obtained QUBO model, as the original formulation of the problem, is NP-hard for classical solver. However, as discussed above, quantum solvers have the potential to overcome the limitations of classical counterparts in this context.

A Simple Example

Consider an Earth observation mission where a single satellite has to acquire images of 4 targets belonging to a region of interest. Suppose that the orbit arc above the region is partitioned into 6 segments and that the orbit segment index sets are the following:

$$\begin{aligned} VTW_1 &= \{1,2\} \\ VTW_2 &= \{2,3,4\} \\ VTW_3 &= \{3,4,5\} \\ VTW_4 &= \{5,6\}, \end{aligned} \tag{8}$$

where the index j has been omitted for simplicity of notation (the formulation contains only one satellite). The mission profit is

$$\begin{aligned} J_P &\doteq \sum_{i\in T}\sum_{k\in VTW_i} w_{ik}\xi_{ik} \\ &= \sum_{i\in T}\sum_{k\in VTW_i} w_{ik}\xi_{ik}^2 \\ &= w_{11}\xi_{11}^2 + w_{12}\xi_{12}^2 \\ &\quad + w_{22}\xi_{22}^2 + w_{23}\xi_{23}^2 + w_{24}\xi_{24}^2 \\ &\quad + w_{33}\xi_{33}^2 + w_{34}\xi_{34}^2 + w_{35}\xi_{35}^2 \\ &\quad + w_{45}\xi_{45}^2 + w_{46}\xi_{46}^2, \end{aligned}$$

where it has be considered that $\xi_{ik} = \xi_{ik}^2$, $\forall i,k$. The following constraints impose that a target is acquired only once:

$$\sum_{k\in VTW_i} \xi_{ik} \le 1, \quad \forall i \in T.$$

That is,

$$\begin{aligned} &\xi_{11} + \xi_{12} \le 1 \\ &\xi_{22} + \xi_{23} + \xi_{24} \le 1 \\ &\xi_{33} + \xi_{34} + \xi_{35} \le 1 \\ &\xi_{45} + \xi_{46} \le 1. \end{aligned}$$

These inequalities give rise to the penalty terms

$$\begin{aligned} \rho_1 &= \xi_{11}\xi_{12} \\ \rho_2 &= \xi_{22}\xi_{23} + \xi_{22}\xi_{24} + \xi_{23}\xi_{24} \\ \rho_3 &= \xi_{33}\xi_{34} + \xi_{33}\xi_{35} + \xi_{34}\xi_{35} \\ \rho_4 &= \xi_{45}\xi_{46}. \end{aligned}$$

In this example, we suppose that all maneuvers are feasible, except the maneuver $(i_1 = 2, k_1 = 4) \to (i_2 = 3, k_2 = 4)$. It follows that

$$\begin{aligned} &F_{23} = \{(4,4)\} \\ &F_{i_1 i_2} = \emptyset, \ (i_1,i_2) \ne (4,4). \end{aligned}$$

The corresponding constraint is

$$\xi_{24} + \xi_{34} \le 1,$$

which corresponds to the penalty term

$$\eta_1 = \xi_{24}\xi_{34}.$$

Finally, we penalize acquisitions requiring a high attitude adjustment and thus a high energy consumption. In particular, we suppose that the acquisition of the 4th target from the 5th segment of the orbit arc requires a significantly larger energy amount with respect to the other acquisitions: $\lambda_{45} \gg \lambda_{ik}, \forall (i,k) \ne (4,5)$. The corresponding penalty term is

$$J_C = \lambda_{45}\xi_{45}.$$

Letting $\Lambda > 0$ be a sufficiently large constant, the objective function to minimize is

$$\begin{aligned} H = &-w_{11}\xi_{11}^2 - w_{12}\xi_{12}^2 \\ &- w_{22}\xi_{22}^2 - w_{23}\xi_{23}^2 - w_{24}\xi_{24}^2 \\ &- w_{33}\xi_{33}^2 - w_{34}\xi_{34}^2 - w_{35}\xi_{35}^2 \\ &+ (\lambda_{45} - w_{45})\xi_{45}^2 - w_{46}\xi_{46}^2 \\ &+ \Lambda(\xi_{11}\xi_{12} + \xi_{24}\xi_{34} + \xi_{45}\xi_{46} \\ &+ \xi_{22}\xi_{23} + \xi_{22}\xi_{24} + \xi_{23}\xi_{24} \\ &+ \xi_{33}\xi_{34} + \xi_{33}\xi_{35} + \xi_{34}\xi_{35}). \end{aligned}$$

This function can be written in the QUBO form (5), where $\zeta = (\zeta_1, \dots, \zeta_{10}) \doteq (\xi_{11}, \xi_{12}, \xi_{22}, \xi_{23}, \xi_{24}, \xi_{33}, \xi_{34}, \xi_{35}, \xi_{45}, \xi_{46}) \in \{0,1\}^{10} \subset \mathbb{N}^{10\times 1}$.

The following $\mathbf{Q}$ matrix is obtained

$$\mathbf{Q} \doteq \begin{bmatrix} -w_{11} & \Lambda & & & & & & & & \\ & -w_{12} & & & & & & & & \\ & & -w_{22} & \Lambda & \Lambda & & & & & \\ & & & -w_{23} & \Lambda & & & & & \\ & & & & -w_{24} & & \Lambda & & & \\ & & & & & -w_{33} & \Lambda & \Lambda & & \\ & & & & & & -w_{34} & \Lambda & & \\ & & & & & & & -w_{35} & & \\ & & & & & & & & \lambda_{45} - w_{45} & \Lambda \\ & & & & & & & & & -w_{46} \end{bmatrix}, \tag{9}$$

where the elements not explicitly indicated are null. A symmetric matrix $\mathbf{Q}$ is then obtained by posing $\mathbf{Q} := (\mathbf{Q} + \mathbf{Q}^T)/2$. The following parameter values are considered: $w_{ik} = 1\ \forall i,k$, $\Lambda = \lambda_{45} = 50$. Since the size of $\mathbf{Q}$ is small, the QUBO problem can be easily solved using a standard algorithm running on a classical computer. Here, the Tabu Search algorithm of Matlab was employed, providing the following result:

$$\xi^* = \begin{bmatrix} \mathbf{1} & \mathbf{0} & 0 & 0 & 0 & 0 \\ 0 & \mathbf{0} & \mathbf{1} & \mathbf{0} & 0 & 0 \\ 0 & 0 & \mathbf{0} & \mathbf{0} & \mathbf{1} & 0 \\ 0 & 0 & 0 & 0 & \mathbf{0} & \mathbf{1} \end{bmatrix}. \tag{10}$$

Note that all rows of ξ^* contain only one entry equal to 1. It means that all targets are captured and they are captured only once. The entries ξ^*_{24} and ξ^*_{34} are null, implying that the forbidden maneuver is not performed (it is sufficient to have just one of these entries equal to 0). We see also that $\xi^*_{45} = 0$, allowing us to avoid the high energy demanding maneuver. In (10), the bold entries individuate the orbit segment index sets (8).

An interesting observation is that the QUBO problem is characterized by several global solutions. Therefore, different results can be obtained running the optimization algorithm several times. In most cases, these results give the same value of the objective function and correspond to different global optima of the problem.

Solvers

This section briefly presents the solver leveraged in this article to solve the closed-loop scheduling of EO satellite formation.

Classical Algorithms

The metaheuristic algorithms selected as classical references in this work are Tabu Search (TS) [31, 35] and Simulated Annealing (SA) [30]. These algorithms have been extensively studied in the literature and are well-suited for solving the QUBO formulation by efficiently exploring the solution space.

The TS algorithm, based on the formulation proposed by Palubeckis [35], uses a short-term memory list to escape local minima when certain conditions are met. The size of the memory list is defined by the tabu tenure parameter. A longer tenure promotes diversification by preventing the search from revisiting the same solutions too quickly, encouraging exploration of different regions in the solution space. The algorithm iterates through the search space, evaluating potential solutions and refining them through a local search to find near-optimal solutions. This process continues until the stopping conditions are met, leading to an approximate optimal solution.

On the other hand, SA is inspired by the metallurgical process of annealing, where a material is heated and then gradually cooled to reach an optimal configuration. Similarly, SA simulates this process on the Hamiltonian of the optimization problem. At each step, a random neighbouring solution is evaluated, and its energy is calculated. Based on the current temperature, the solution may be accepted or rejected. The temperature governs the exploration of the solution space: higher temperatures encourage broader exploration but may accept suboptimal solutions. The process continues iteratively, with the temperature gradually decreasing until it reaches zero.

Quantum Annealers

There are two primary approaches to exploit quantum computers in optimization: quantum circuit model quantum computing [36, 37] and adiabatic quantum computation (AQC) [38]. In the quantum circuit model, computation is performed by applying a series of unitary gates to a set of quantum bits (qubits), which are measured at the end of the computation to develop various algorithms, including optimization ones. Conversely, in AQC, an initial multi-qubit quantum state is prepared as the ground state of a simple Hamiltonian. This state undergoes an adiabatic time evolution, transforming the system into a final Hamiltonian whose ground state represents the solution to an optimization problem. Between these two approaches, the present work focuses on AQC and in particular on the Quantum Annealing paradigm, which exploits the adiabatic principle to solve optimization problems [39–41].

Quantum Annealers (QAs) are special-purpose quantum computers designed to efficiently solve QUBO problems, such as (7), providing a significant computational speedup compared to classical computers [42, 43], while also potentially enhancing solution quality. Now, we provide an overview of quantum annealers and their operating principles. Defining

$$\sigma = (\sigma_1, \dots, \sigma_n) \doteq 2\zeta - I \in \{-1, 1\}^n \subset \mathbb{Z}^{n\times 1},$$

the QUBO function can be written as

$$\begin{aligned} H = \zeta^\top \mathbf{Q}\, \zeta &= \frac{1}{4}(\sigma + I)^\top \mathbf{Q}\, (\sigma + I) \\ &= \frac{1}{4}\sigma^\top \mathbf{Q}\sigma + \frac{1}{2} I^\top \mathbf{Q}\sigma + \frac{1}{4} = H_F + \frac{1}{4}, \end{aligned}$$

where the function H_F—called transverse-field Ising Hamiltonian—is defined as

$$H_F \doteq \sigma^\top J_F \sigma + h_F \sigma, \quad J_F \doteq \frac{1}{4}\sigma^\top \mathbf{Q}, \quad h_F \doteq \frac{1}{2} I^\top \mathbf{Q}, \tag{11}$$

and represents the energy of a physical system consisting of n interacting particles, described by two-state variables $\sigma_i, i = 1, \dots, n$ (e.g., spin of electrons, polarization of photons, superconducting loops, etc.). A Quantum Annealer (QA) operates as a lattice of n interacting nodes, known as qubits, each also described by two-state variables but governed by the laws of quantum mechanics. These qubits

are physically realized using superconducting loops [41, 44]. Unlike classical bits, which can exist in only one of two distinct states, a qubit can exist in a superposition of states. This unique characteristic of quantum systems enables quantum parallelism, allowing the QA to explore multiple solutions to a problem at the same time, in contrast to classical computers, which examine one solution at a time. This quantum parallelism is a defining advantage of QAs. Another critical feature of QAs is quantum tunneling, which allows the system to bypass energy barriers and reduces the chance of remaining trapped in local optima, as illustrated in Fig. 5c. Together, these features—quantum parallelism and quantum tunneling—make QAs particularly effective for solving optimization problems. The main steps involved in using a QA to solve a QUBO-like problem are outlined below.

Quantum Annealing Process

1. *Initialization:* The QA system is initialized in a superposition of states, representing all the possible configurations of the optimization problem. Therefore, each qubit is in a superposition of its basis state $|0\rangle$ and $|1\rangle$, which is the ground state of the initial Hamiltonian, indicated as H_I. This can be visualized as the spins aligned on the x-axis of Fig. 5a or the flat bottom of the tank in the hydraulic model usually exploited for explaining QA system evolution of Fig. 5b.
2. *Adiabatic evolution:* The Hamiltonian evolves continuously from H_I, whose ground state is easily prepared, to the final Hamiltonian H_F in (11), which encodes the optimization problem. This evolution follows an adiabatic process, ensuring that the QA system remains in the ground state throughout the transformation, also

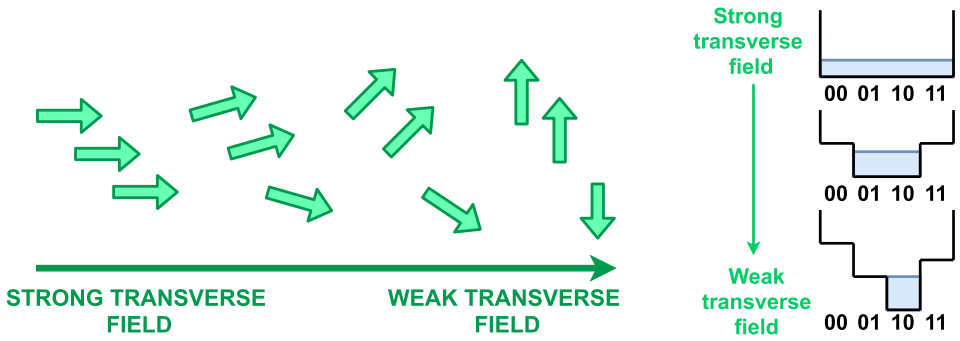

(a) Spins evolution during annealing. When a strong transverse field is applied, spins are in a superposition state. Reducing the transverse field, spins assume a spin-down or spin-up state to reach the lowest energy configuration.

(b) Quantum annealer system evolution explained through an *hydraulic model*.

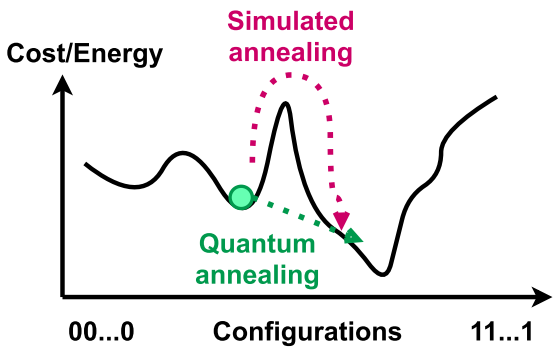

(c) Quantum tunneling *vs.* thermal climbing. The first represents the exploration mechanism of quantum annealing, while the second that of simulated annealing.

Fig. 5 Overview of quantum annealing

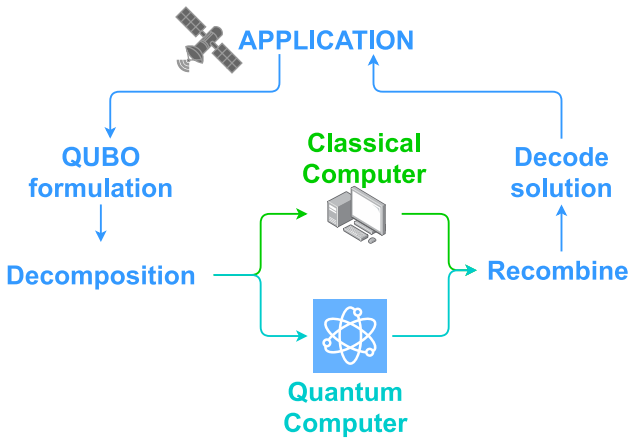

Fig. 6 Hybrid quantum computer

avoiding local minima thanks to quantum tunneling. The evolution is described by $H_{QA} = \varphi(t)H_I + (1 - \varphi(t))H_F$, where H_{QA} is the QA Hamiltonian and $\varphi(t)$ is a continuous function of time such that $\varphi(0) = 1$ and $\varphi(T_A) = 0$, being $T_A > 0$ called the annealing time. This process can be graphically represented in Fig. 5b as the gradual deformation of the tank's bottom to represent the objective function, with water flowing to the lowest points. Alternatively, it can be represented as spins of Fig. 5a gradually reorienting to achieve the lowest energy configuration.

3. *Measurement:* Once the evolution process is complete, the final spin vector σ^* is measured. This vector corresponds to a minimum of the Hamiltonian, where $H_F = H - 1/4$. Consequently, the solution to the QUBO problem (7) is $\zeta^* = (\sigma^* + I)/2$.
4. *Post-processing:* The obtained solution might not be perfect due to noise and defects in the quantum hardware. Post-processing techniques like classical optimization algorithms can be applied to refine the solution (e.g., simulated annealing or tabu search).
5. *Repetitions:* The whole procedure (steps 1–4) can be repeated multiple times and the best result is selected. □

After the initialization step, the system operates in a superposition state, enabling simultaneous and parallel exploration of the solution space. This provides an exponential speedup compared to classical methods, where solutions must be evaluated sequentially. However, the evolution from the initial to the final Hamiltonian cannot be arbitrarily fast. The Adiabatic Theorem states that a quantum system starting from a ground state persists in a ground state, provided that the change in time of the Hamiltonian is sufficiently slow. Let T_A be the annealing time, i.e., the time taken to change the Hamiltonian from H_I to H_F. The theorem implies that the system remains in the ground state if:

$$T_A \geq \frac{1}{\min_{t\in[0,T_A]} \Delta E(t)^2}, \tag{12}$$

where ΔE is the gap between the two lowest energy levels of the QA system. The combination of the exponential speedup in the initialization step and the limit imposed by the Adiabatic Theorem yields, in any case, a significant computational complexity reduction with respect to classical computers. Indeed, although it is notoriously difficult to analyze the runtime of adiabatic optimization algorithms, several works in the literature show that a quadratic speedup with respect to classical computers can be guaranteed [42, 43].

Failure to satisfy (12) introduces a probability of jumping to higher energy states, yielding sub-optimal solutions. This gives rise to a trade-off between computational speed and quality of the solution: sub-optimal solutions can be found, which require a shorter annealing time with respect to an optimal solution but are satisfactory in practice. Moreover, the complexity of estimating the required annealing time exceeds that of solving the problem itself, making complex to define the evolution time. Current quantum devices do not support such extended computation times, as the time required for the operations influences the noise, compromising the system's performance.

A leading company in the field of QAs is D-Wave Systems [45], which develops QAs with a growing number of qubits (more than 5000), enabling the solution of increasingly complex optimization problems. Despite the significant implications of the Adiabatic Theorem, practical challenges such as thermal fluctuations and background noise make it difficult to perfectly satisfy the slow rate of change requirement. Consequently, QA is often seen as a relaxation of purely adiabatic quantum computing, where heuristic parameters govern the annealing schedule, allowing non-zero probabilities of leaving the ground state.

Hybrid Quantum Annealing (HQA) offers an alternative approach, addressing many challenges associated with directly working with the quantum processing unit (QPU).

Table 1 OE for the satellite constellation

ID	a (km)	i (°)	Ω (°)	e	ω (°)	ν (°)
1000	6903.67	97.58	97.85	16.55e−4	130.99	2.03
2000	6909.06	97.58	93.20	9.97e−4	254.46	155.23
3000	6898.60	97.58	92.36	14.60e−10	276.73	140.19

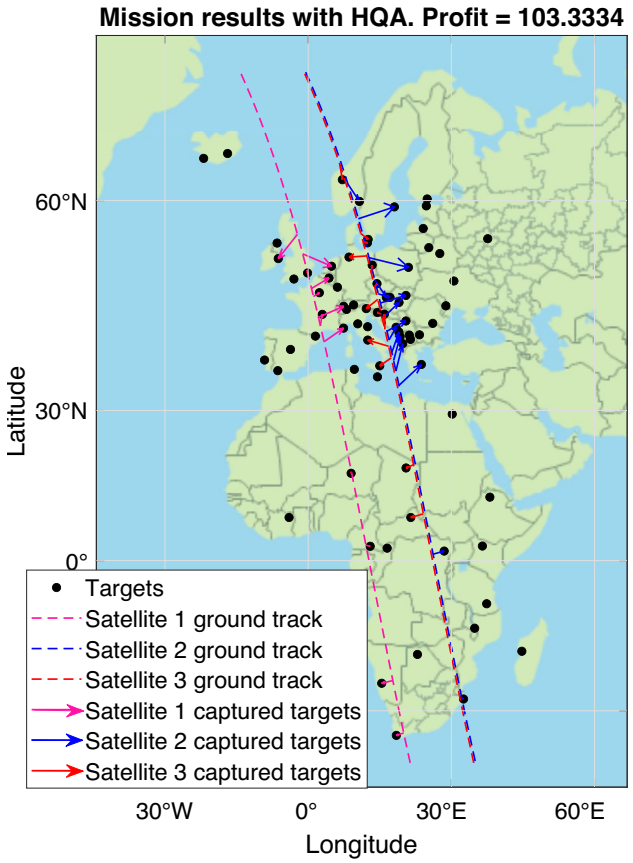

Fig. 7 Captured targets over Europe and Africa

For instance, the selection of weights for constraints (couplings) and profits (biases) when formulating the QUBO problem is critical. Incorrect weights can lead to small energy gaps, increasing the likelihood of transitioning to higher energy states, or excessively large weights, which hinder adequate exploration of the search space. Additionally, embedding logical qubits onto physical qubits introduces challenges such as chain breaks, potentially resulting in invalid solutions. Even with automated tools like auto-scaling from samplers, parameter calibration remains demanding.

The hybrid approach mitigates these difficulties by combining heuristic and quantum techniques, as shown in Fig. 6. Large or complex problems are divided into smaller subproblems, which are mapped to the QPU. The results are then combined to form a comprehensive solution. This approach automates back-end configurations and embedding, ensuring no miscalibration. During a set time limit, heuristic solvers analyze the QUBO matrix, working in parallel to identify acceptable solutions. When needed, these solvers utilize the QPU, integrating quantum outputs to refine the global response. This hybrid framework enhances both scalability and reliability, making QA applicable to real-world problems.

Mission Scenario Description

In order to test and validate the proposed algorithm and expand upon the proposed dataset in [28], a realistic scenario is considered. It includes a list of most of the World Capitals, ensuring that the targets are well-distributed. The main characteristics of the scenario are shown below:

1. Number of decision variables: 7731.
2. Number of unique targets: 166.
3. Constraint density: 18.21%.

A pre-treatment phase, however, is necessary as this data must be prepared to serve as input for the QUBO problem formulation. Generally, in a nominal operation, the client provides a list of desired targets, characterized by their latitude, longitude and altitude (LLA) coordinates, duration and priority. This data must be analyzed and subsequently integrated with the propagated orbits in order to generate the input files for the problem formulation. An algorithm is developed with MATLAB so the VTW's of each S/C with respect to every target are generated. This procedure starts by firstly importing the target list and the satellite orbital elements (OE), and calculating its propagated orbit in particular frames of reference. Accordingly, for one orbital evolution, a discretization time of one second is chosen so that the generated data is accurate enough. The pre-treatment phase is performed with an iteration loop that verifies if the current time slot is identified as a valid observation opportunity in the target's VTW. As this procedure is done for all targets and satellites, text files with useful information are generated with a unique mission identifier, ending the pre-processing phase.

To accomplish this mission, three satellites have been taken into account. Their parameters, presented in Table 1, are based on the well-documented SuperView-1 constellation consisting of Chinese commercial and remote sensing satellites [32], launched in 2018. Their agile nature is accounted for by allowing maneuvers in the roll and pitch directions, with a range of $\pm 45°$, for both angles.

The first column shows the unique ID of the S/Cs, while the OE are presented from columns 2 to 7, respectively:

Table 2 Comparison between classic and hybrid quantum algorithms for the small-scale dataset

	Mean pract. profit $-H$	SD pract. profit $-H$	Mean runtime (s)	SD runtime (s)
TS	90.76	1.07	6.96	1.31
SA	99.23	0.74	25.46	2.83
HQA	101.94	0.37	4.0140	0.0038

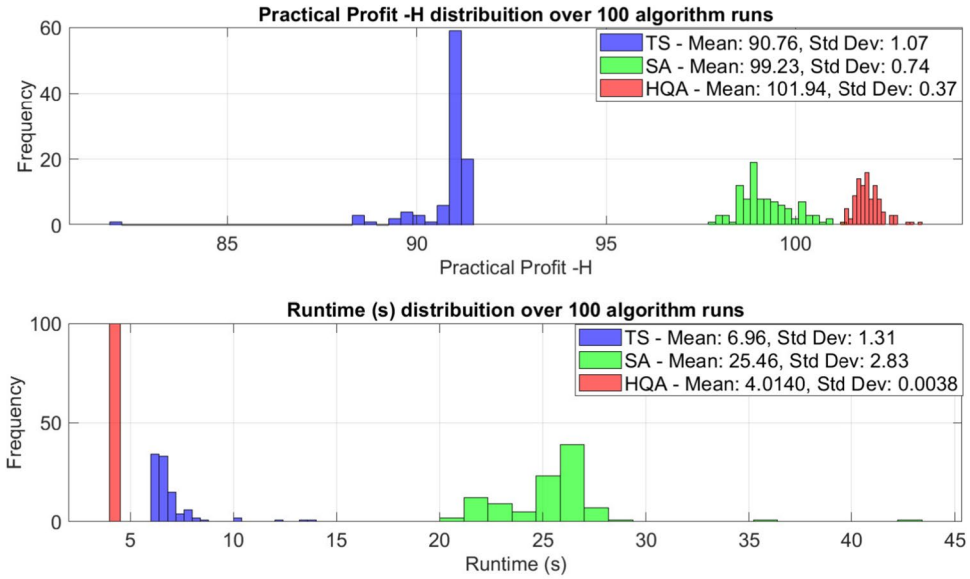

Fig. 8 Results distribution for the small-scale scenario

semi-major axis a, inclination i, right ascension of the ascending node Ω, eccentricity e, argument of perigee ω and mean anomaly ν. From the original specifications, the OE for satellite 1, with ID 1000, is slightly modified to fit the generated data requirements for sparsity. These OE account for heliosynchronous, highly polar and almost circular orbits. One orbital revolution for the constellation is around 95 min.

The chosen profit, from 1 to 5, and duration are arbitrarily selected to be as generic as possible while still preserving the realistic nature of the problem. In practice, the downsampled data are used for the problem formulation, considerably reducing the number of variables, but still maintaining the system's physical characteristics and real-world applicability [32]. Some authors prefer a finer resolution [46], while others [47] opt for an even greater time step. It should be noted that this scenario consists of a high-density dataset due to the close vicinity and the number of targets. Indeed, satellites two and three may observe more than 30 targets in less than 20 min with many overlapping VTWs. Consequently, the resulting $\mathbf{Q}$ matrix is highly dense, making the problem hard to solve, especially with QA, as it requires more physical qubits to embed the variable relations.

Simulation Results

In this section, the proposed quantum algorithm is validated and compared with the following classical meta-heuristic algorithms: Tabu Search (TS) [31] and Simulated Annealing (SA) [30]. First, an open-loop scheduling approach is considered, applying it to scenarios with both a limited number of targets and a larger set of targets. Subsequently, a closed-loop scheduling approach is presented.

Open-Loop Scheduling

The tests conducted in this study involved the implementation of the proposed strategies using Matlab for obtaining the QUBO formulation. Then, depending on the strategy used, these QUBO problems were solved using different solvers provided by D-Wave. In particular: (i) the `D-Wave Leap Hybrid Sampler` for the HQA, (ii) the `D-Wave SimulatedAnnealingSampler` for the SA, and (iii) the `D-Wave TabuSampler` for the TS.

Note that, before deciding to use the HQA, a thorough comparison was conducted with pure QA, finding that nowadays the latter is not able to produce satisfactory solutions for large-scale problems. This is due to the known problems of the current quantum hardware, such as environmental noise, a limited number of physical qubits, and intricate problem-embedding strategies.

Small-Scale Scheduling Problem

Here, the results obtained in [28] are briefly resumed. In that paper, a list of all the European capitals and many UNESCO Natural World Heritage sites was considered (see Fig. 7). To evaluate the performance, the algorithms under consideration were executed 100 times in order to obtain a comparative distribution analysis. The evaluation metrics included: (i) the mean value of the Practical Profit $-H$ (Mean Pract. Profit $-H$), (ii) its standard deviation (SD Pract. Profit $-H$), (iii) the mean value of the Runtime (Mean Runtime), and iii) its standard deviation (SD Runtime). Considering the best outcome of the 100 executions of the HQA, a maximum Practical Profit of 103.33 was obtained with 40 unique targets captured. This result is visually depicted in Fig. 7. Table 2 collects the the average values, computed over the

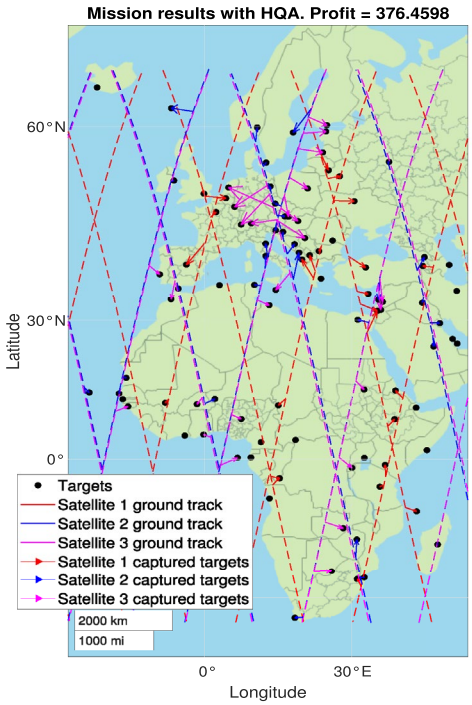

(a) Captured targets over Europe and Africa.

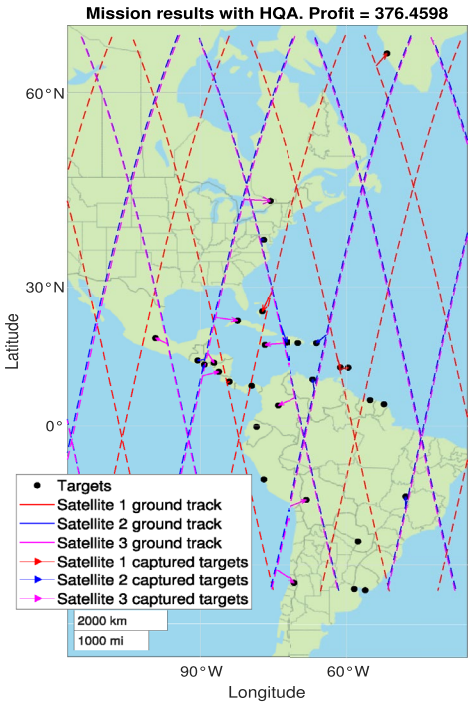

(b) Captured targets over North and South America.

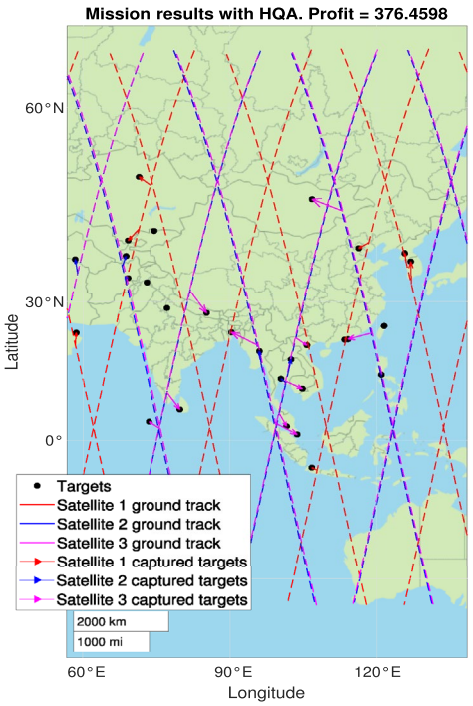

(c) Captured targets over Asia and Oceania.

Fig. 9 AEO scheduling problem with HQA for the large-scale dataset

Table 3 Comparison between classic and hybrid quantum algorithms for the large-scale dataset

	Mean pract. profit $-H$	SD pract. profit $-H$	Mean runtime (s)	SD runtime (s)
SA	369.03	1.44	445.88	3.79
HQA	372.76	1.53	28.4158	0.0358

100 runs, of both the mean and the standard deviation for each performance metric across of the three algorithms. Additionally, Fig. 8 shows the corresponding comparative distribution. The results clearly demonstrate that HQA consistently outperforms its classical counterparts. Notably, it not only achieves higher average practical profit and lower average runtime, but also yields reduced standard deviation values for both metrics, indicating greater reliability and robustness. These findings highlight the effectiveness of HQA as a more stable and efficient solution approach for the small-scale scheduling problem.

Large-Scale Scheduling Problem

Based on the results obtained in [28], this paper extends the analysis by addressing a daily scheduling problem. This extension is valuable for assessing how both classical and quantum algorithms scale in complexity as the problem size increases.

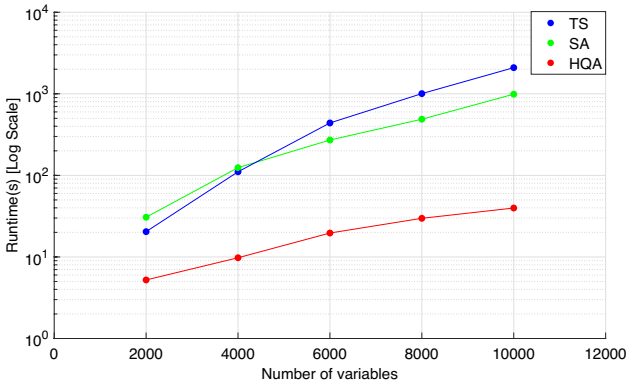

Fig. 11 Runtime as a function of the number of variables

Taking into account the characteristics of the scenario described in Sect. 5, it can be noted that, while the targets are relatively densely distributed geographically, the resulting matrix exhibits only around 18% constraint density. Nevertheless, as the number of decision variables increases, the complexity of solving the problem grows significantly. To evaluate the performance, the algorithms under consideration were executed 50 times in order to obtain a comparative distribution, using the same metrics as in the previous analysis. In the best outcome of 50 executions of the HQA, a maximum Practical Profit of 376.4598 was obtained, with 140 unique targets captured. This result is visually depicted in Fig. 9.

Table 3 reports the average values, computed over 50 runs, of both the mean and the standard deviation for each

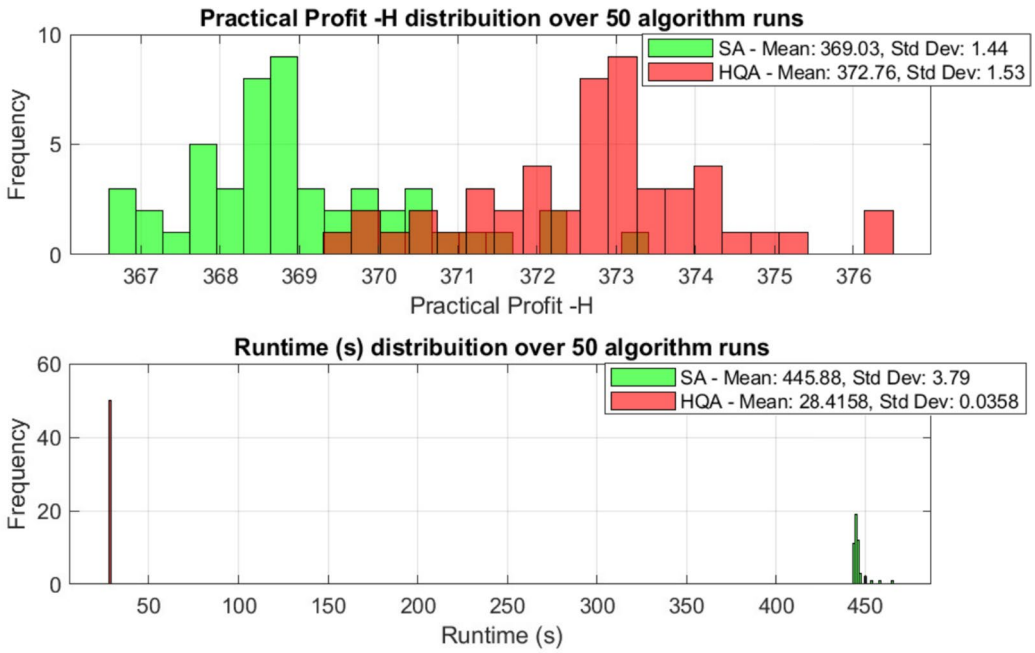

Fig. 10 Results distribution for the large-scale scenario

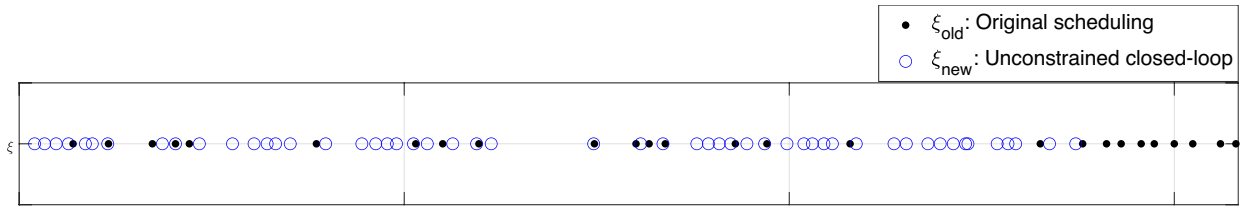

(a) Unconstrained closed-loop scenario.

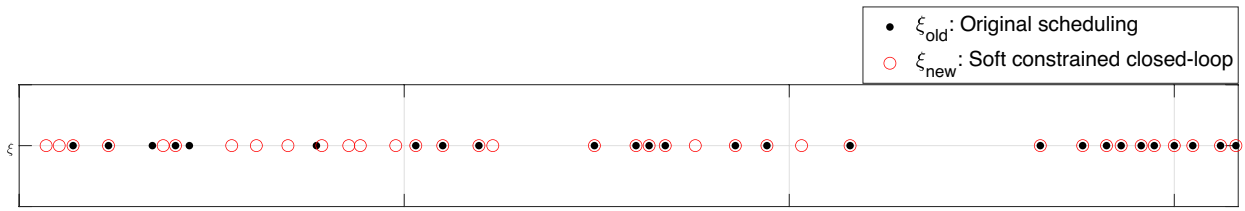

(b) Soft constrained closed-loop scenario.

Fig. 12 Closed-loop reprogrammed schedule: comparison between constrained and unconstrained cases. The constrained scheduling retains a higher overlap between the targets of the old and new schedules, with only 3 discrepancies compared to 17 in the unconstrained case

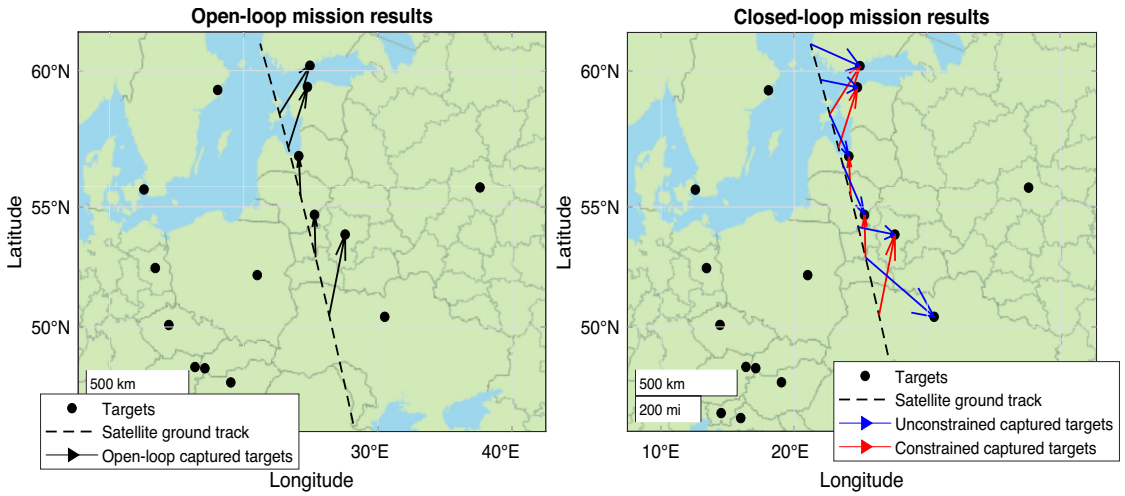

(a) Open-loop scenario. (b) Closed-loop scenario.

Fig. 13 Local projection for constrained and unconstrained cases

performance metric of the three algorithms. It is important to note that TS was excluded from this analysis due to its lack of competitive performance for large-scale problems. Both SA and HQA yield viable and feasible mission results with comparable Practical Profit $-H$ values and, most importantly, without any constraint violation. A clear advantage of the HQA can be noted in terms of runtime. On average, it is approximately 15.7 times faster than the SA.

Additionally, from the outcomes of the 50 runs, a comparative distribution is presented in Fig. 10. The HQA is considerably better than its classical counterpart in terms of mean value and standard deviation regarding runtime, and offers similar results for the practical profit. These remarkable results were obtained using around 85 ms of QPU access time with respect to the 28 s of total runtime, showing the effectiveness of combining the classical meta-heuristics with quantum methods.

This large-scale scenario demonstrates that, as the problem size increases, quantum algorithms can significantly outperform classical algorithms, both in terms of computational

efficiency and solution quality. This is a crucial finding, showcasing the practical viability of quantum algorithms for such mission scenarios. To analyze how the computational time of HQA scales with problem size, we have performed a series of tests varying the number of variables and comparing the results with those obtained using SA and TS. As shown in Fig. 11,[2] the runtime of HQA increases at a significantly slower rate than that of the classical approaches. This leads to substantial advantages, potentially by several orders of magnitude, as the number of variables grows, therefore highlighting its superior scalability and efficiency in handling large-scale problems. Therefore, the hybrid approach is particularly well suited for real-time, closed-loop scheduling applications, as discussed below.

Closed-Loop Scheduling

Here, the results obtained in the case of rescheduling are presented. To show the effectiveness of the soft constraint in penalizing deviations from the original scheduling results, a simulated unexpected event is introduced. This event, which could represent a mechanical defect or a subsystem malfunction, forces the formation into safe mode and triggers the need for a new schedule. A profit variation of 20% is applied to a subset of the dataset, after the trigger event, simulating natural changes that may occur in a period of 24 h.

A comparison between the constrained and unconstrained cases highlights the efficacy of the soft constraint. In Fig. 12, black markers illustrate the positions on the original scheduling binary vector where an acquisition was performed, while blue and red circles represent the new observation instants after the rescheduling. If the penalty function is not applied, Fig. 12a reveals that the optimization process converged to an entirely new minimum. In contrast, new acquisitions tend to follow the original results in the constrained case, as shown in Fig. 12b. Notably, the constrained scheduling retains a higher overlap between the targets of the old and new schedules, with only 3 discrepancies compared to 17 in the unconstrained case. This alignment reduces the rescheduling cost and maintains consistency with the original plan, demonstrating the effectiveness of the penalty function in minimizing deviations.

To provide a detailed illustration of the responsiveness of the closed-loop scheduling approach to an emergency event, we analyze a subset of the scenario depicted in Fig. 12, focusing on a specific region in Europe. In this context, Fig. 13a presents the original schedule, while Fig. 13b compares the rescheduling outcomes with and without the incorporation of the proposed penalty.

Conclusions

In conclusion, this paper introduces a closed-loop QUBO formulation for the AEOSs scheduling problem. This formulation has been implemented onto the real D-Wave quantum computer using the HQA approach and compared with classical optimization solvers, such as the SA and the TS. The obtained results show improved performance in terms of both quality of the solutions and computational times, suggesting that hybrid techniques can handle a one-day scheduling horizon, effectively simulating real missions. We could observe that, as the problem size grows, classical algorithms experience a significant degradation in performance. While HQA already showed faster performance for the smaller test dataset, its advantage became even more pronounced as the problem scaled to larger, real-world scenarios. This trend highlights the exponential growth in solving time for classical algorithms as the size of the NP-hard problem increases, whereas the hybrid approach demonstrated significantly better scalability, showing slower performance degradation with larger problem sizes. These findings demonstrate the strong potential of quantum computing to tackle large-scale scheduling problems that are otherwise challenging for classical methods. By incorporating a soft constraint for the closed-loop rescheduling, the proposed approach effectively handled unexpected S/C fault events, ensuring that the new schedule remained as close as possible to the original. Finally, it is important to note that the current quantum devices are limited in terms of number of qubits availability, connectivity and fidelity. These limitations necessitate the use of hybrid solvers for contemporary industrial applications.

While our work highlights the current limitations of quantum annealing hardware, particularly about scalability, it is important to note that ongoing advancements in quantum annealers—such as increased qubit count, improved coherence, and expanded connectivity—are expected to significantly enhance their applicability. For instance, D-Wave's hardware has evolved in the last few years from the 6-qubit connectivity of the Chimera topology to the 20-qubit connectivity of the Zephyr architecture, and from 128 qubits in the D-Wave One system to over 5000 qubits in the latest Advantage devices. Moreover, D-Wave has declared a clear development roadmap[3] aimed at enabling higher-dimensional connectivity and introducing fault-tolerant features, which may further generalize quantum annealing approaches to a wider class of optimization problems. Therefore, despite the constraints of current-generation devices, the results obtained are promising and represent a meaningful step forward in the application of quantum annealing to real-world problems. Indeed, they demonstrate that exploring quantum

[2] The time scale in the figure is logarithmic.

[3] https://www.dwavequantum.com/media/xvjpraig/clarity-roadmap_digital_v2.pdf.

solutions can provide valuable insights for the future of real-time satellite scheduling research.

Future Works

Regarding future improvements, the proposed formulation could be further refined by relaxing the model constraints to enhance its applicability across a broader range of scenarios. Additionally, incorporating an integer-valued unicity constraint to allow multiple target acquisitions could be beneficial for specific applications. For the closed-loop application, alternative soft constraints could be formulated to accommodate new unexpected events, such as high cloud coverage, storms, or a change in priorities for surveillance over specific areas due to geopolitical developments. Finally, a reconfigurable model for movable targets could optimize both orbital adjustments and target acquisition. For what concerns the QUBO solving, other quantum or quantum-inspired approaches, like Grover Adaptive Search [48, 49], variational quantum algorithms [50, 51] and Simulated Quantum Annealing [52, 53], could be explored in the next future to evaluate their solutions.

Acknowledgements We would like to thank D-Wave Systems for providing access to their quantum annealer through the Leap Quantum LaunchPad program.

Author Contributions Conceptualization, all authors; methodology, all authors; software, V.M; validation, V.M, M.B., and D.V.; formal analysis, V.M, M.B., and D.V.; writing—original draft preparation, V.M, M.B., D.V., and C.N.; writing—review and editing, all authors; supervision, C.N.; project administration, C.N. All authors have read and agreed to the published version of the manuscript.

Funding Open access funding provided by Politecnico di Torino within the CRUI-CARE Agreement. This research received no specifc grant from any funding agency in the public, commercial, or not for proft sectors. The authors declare they have no financial interests.

Data Availability The datasets generated during and/or analyzed during the current study are available from the corresponding author on reasonable request.

Declarations

Conflict of Interest The authors declared that they have no conflict of interest to this work.

Research Involving Human and/or Animals Not applicable.

Consent for Publication All authors have consented to the publication of this manuscript.

References

1. Anderson K, Ryan B, Sonntag W, Kavvada A, Friedl L. Earth observation in service of the 2030 agenda for sustainable development. Geo-spat Inform Sci. 2017;20(2):77–96.
2. Zhao Q, Yu L, Du Z, Peng D, Hao P, Zhang Y, Gong P. An overview of the applications of earth observation satellite data: impacts and future trends. Remote Sens. 2022;14(8):1863.
3. Ruf C, Unwin M, Dickinson J, Rose R, Rose D, Vincent M, Lyons A. CYGNSS: enabling the future of hurricane prediction [remote sensing satellites]. IEEE Geosci Remote Sens Mag. 2013;1(2):52–67.
4. Hirschmugl M, Gallaun H, Dees M, Datta P, Deutscher J, Koutsias N, Schardt M. Methods for mapping forest disturbance and degradation from optical earth observation data: a review. Curr For Rep. 2017;3:32–45.
5. Chuvieco E, Mouillot F, van der Werf GR, San Miguel J, Tanase M, Koutsias N, García M, Yebra M, Padilla M, Gitas I, Heil A, Hawbaker TJ, Giglio L. Historical background and current developments for mapping burned area from satellite earth observation. Remote Sens Environ. 2019;225:45–64.
6. Guo H-D, Zhang L, Zhu L-W. Earth observation big data for climate change research. Adv Clim Change Res. 2015;6(2):108–117. Special issue on advances in Future Earth research.
7. Dolce F, Di Domizio D, Bruckert D, Rodríguez A, Patrono A. In: Schrogl K-U, editor. Earth Observation for security and defense. Cham: Springer; 2020. p. 705–31.
8. Verfaillie G, Lemaître M. Selecting and scheduling observations for agile satellites: some lessons from the constraint reasoning community point of view. In: International Conference on Principles and Practice of Constraint Programming. Springer, Berlin, Heidelberg, pp 670–684; 2001.
9. Wang X, Wu G, Xing L, Pedrycz W. Agile earth observation satellite scheduling over 20 years: formulations, methods, and future directions. IEEE Syst J. 2021;15(3):3881–92.
10. Brucker P. Scheduling algorithms. J Oper Res Soc. 1999;50:774.
11. Globus A, Crawford J, Lohn J, Pryor A. Scheduling earth observing satellites with evolutionary algorithms. In: International conference on space mission challenges for information technology. Pasadina; 2003.
12. Wang J, Jing N, Li J, Chen ZH. A multi-objective imaging scheduling approach for earth observing satellites. In: Proceedings of the 9th annual conference on genetic and evolutionary computation. GECCO '07. New York: Association for Computing Machinery; 2007. p. 2211–8.
13. Baek S-W, Han S-M, Cho K-R, Lee D-W, Yang J-S, Bainum PM, Kim H-D. Development of a scheduling algorithm and GUI for autonomous satellite missions. Acta Astronaut. 2011;68(7):1396–402.
14. Pemberton JC, Greenwald L. On the need for dynamic scheduling of imaging satellites. Int Arch Photogramm Remote Sens Spat Inf Sci. 2002;34(1):165–71.
15. Dishan Q, Chuan H, Jin L, Manhao M. A dynamic scheduling method of earth-observing satellites by employing rolling horizon strategy. Sci World J. 2013;2013(1): 304047.

16. Niu X, Tang H, Wu L, Deng R, Zhai X. Imaging-duration embedded dynamic scheduling of earth observation satellites for emergent events. Math Probl Eng. 2015;2015(1): 731734.
17. Roland J, Cerf NJ. Quantum search by local adiabatic evolution. Phys Rev A. 2002;65(4): 042308.
18. Albash T, Lidar DA. Demonstration of a scaling advantage for a quantum annealer over simulated annealing. Phys Rev X. 2018;8: 031016.
19. Stollenwerk T, O'Gorman B, Venturelli D, Mandrà S, Rodionova O, Ng H, Sridhar B, Rieffel EG, Biswas R. Quantum annealing applied to de-conflicting optimal trajectories for air traffic management. IEEE Trans Intell Transp Syst. 2020;21(1):285–97.
20. Inoue D, Okada A, Matsumori T, Aihara K, Yoshida H. Traffic signal optimization on a square lattice with quantum annealing. Sci Rep. 2021;11(1):3303.
21. Morstyn T. Annealing-based quantum computing for combinatorial optimal power flow. IEEE Trans Smart Grid. 2023;14(2):1093–102.
22. Irbäck A, Knuthson L, Mohanty S, Peterson C. Using quantum annealing to design lattice proteins. Phys Rev Res. 2024;6: 013162.
23. Marchesin A, Montrucchio B, Graziano M, Boella A, Mondo G. Improving urban traffic mobility via a versatile quantum annealing model. IEEE Trans Quantum Eng. 2023;4:1–13.
24. Volpe D, Cirillo GA, Fantini R, Boella A, Mondo G, Graziano M, Turvani G. Quantum-compliant users scheduling optimization in joint transmission mobile access networks. Quantum Inf Process. 2024;23(7):262.
25. Mattesi M, Asproni L, Mattia C, Tufano S, Ranieri G, Caputo D, Corbelletto D. Financial portfolio optimization: a QUBO formulation for Sharpe ratio maximization. Technical report. 2023.
26. Novara C, Boggio M, Volpe D. A quantum optimization approach to Nonlinear Model Predictive Control. In: European Control Conference (ECC); 2025.
27. Stollenwerk T, Michaud V, Lobe E, Picard M, Basermann A, Botter T. Agile earth observation satellite scheduling with a quantum annealer. IEEE Trans Aerosp Electron Syst. 2021;57(5):3520–8.
28. Marchioli V, Boggio M, Volpe D, Massotti L, Novara C. Scheduling of satellite constellation operations in EO missions using quantum optimization. In: International conference on optimization, learning algorithms and applications. Berlin: Springer; 2024. p. 227–42.
29. Booth M, Reinhardt SP, Roy A. Partitioning optimization problems for hybrid classical/quantum execution. Technical Report, 01–09. 2017.
30. Kirkpatrick S, Gelatt CD, Vecchi MP. Optimization by simulated annealing. Science. 1983;220(4598):671–80.
31. Glover F. Tabu search: a tutorial. Interfaces. 1990;20(4):74–94.
32. Wang X, Han C, Zhang R, Gu Y. Scheduling multiple agile earth observation satellites for oversubscribed targets using complex networks theory. IEEE Access. 2019;7:110605–15.
33. Albash T, Lidar DA. Demonstration of a scaling advantage for a quantum annealer over simulated annealing. Phys Rev X. 2018;8(3): 031016.
34. Glover F, Kochenberger G, Du Y. A tutorial on formulating and using QUBO models. 2018. arXiv preprint. arXiv:1811.11538.
35. Palubeckis G. Multistart tabu search strategies for the unconstrained binary quadratic optimization problem. Ann Oper Res. 2004;131:259–82.
36. Barenco A, Bennett CH, Cleve R, DiVincenzo DP, Margolus N, Shor P, Sleator T, Smolin JA, Weinfurter H. Elementary gates for quantum computation. Phys Rev A. 1995;52:3457–67.
37. Volpe D, Orlandi G, Turvani G. Improving the solving of optimization problems: a comprehensive review of quantum approaches. Quantum Rep. 2025;7(1):3.
38. Albash T, Lidar DA. Adiabatic quantum computation. Rev Mod Phys. 2018;90: 015002.
39. Morita S, Nishimori H. Mathematical foundation of quantum annealing. J Math Phys. 2008;49(12): 125210.
40. Kadowaki T, Nishimori H. Quantum annealing in the transverse Ising model. Phys Rev E. 1998;58(5):5355.
41. Johnson MW, Amin MH, Gildert S, Lanting T, Hamze F, Dickson N, Harris R, Berkley AJ, Johansson J, Bunyk P, et al. Quantum annealing with manufactured spins. Nature. 2011;473(7346):194–8.
42. Boixo S, Ortiz G, Somma R. Fast quantum methods for optimization. Eur Phys J Spec Top. 2015;224(1):35–49.
43. Zanca T, Santoro GE. Quantum annealing speedup over simulated annealing on random Ising chains. Phys Rev B. 2016;93: 224431.
44. Hauke P, Katzgraber HG, Lechner W, Nishimori H, Oliver WD. Perspectives of quantum annealing: methods and implementations. Rep Prog Phys. 2020;83(5): 054401.
45. D-Wave Systems. https://www.dwavesys.com/. Accessed 12 Jan 2024.
46. Peng G, Song G, Xing L, Gunawan A, Vansteenwegen P. An exact algorithm for agile earth observation satellite scheduling with time-dependent profits. Comput Oper Res. 2020;120: 104946.
47. Liu X, Laporte G, Chen Y, He R. An adaptive large neighborhood search metaheuristic for agile satellite scheduling with time-dependent transition time. Comput Oper Res. 2017;86:41–53.
48. Giuffrida L, Volpe D, Cirillo GA, Zamboni M, Turvani G. Engineering Grover adaptive search: exploring the degrees of freedom for efficient QUBO solving. IEEE J Emerg Sel Top Circuits Syst. 2022;12(3):614–23.
49. Gilliam A, Woerner S, Gonciulea C. Grover adaptive search for constrained polynomial binary optimization. Quantum. 2021;5:428.
50. Farhi E, Goldstone J, Gutmann S. A quantum approximate optimization algorithm. 2014. arXiv preprint. arXiv:1411.4028.
51. Tilly J, Chen H, Cao S, Picozzi D, Setia K, Li Y, Grant E, Wossnig L, Rungger I, Booth GH, et al. The variational quantum eigensolver: a review of methods and best practices. Phys Rep. 2022;986:1–128.
52. Crosson E, Harrow AW. Simulated quantum annealing can be exponentially faster than classical simulated annealing. In: 2016 IEEE 57th annual symposium on foundations of computer science (FOCS); New Brunswick, NJ, USA. IEEE; 2016. p. 714–23.
53. Volpe D, Cirillo GA, Zamboni M, Turvani G. Integration of simulated quantum annealing in parallel tempering and population annealing for heterogeneous-profile QUBO exploration. IEEE Access. 2023;11:30390–441.